Available online at www.sciencedirect.com
SCIENCE DIRECT®
Journal of Organometallic Chemistry 689 (2004) 50–57
Journal of Organometallic Chemistry
www.elsevier.com/locate/jorganchem

Mixed-metal cluster chemistry. 26 [1]. Proclivity for "all-terminal" or "plane-of-bridging-carbonyls" ligand disposition in tungsten–triiridium clusters

Alistair J. Usher [a], Gulliver T. Dalton [a], Nigel T. Lucas [a], Susan M. Waterman [a], Simon Petrie [a], Robert Stranger [a], Mark G. Humphrey [a,*], Anthony C. Willis [b]

[a] Department of Chemistry, Australian National University, Canberra, ACT 0200, Australia
[b] Research School of Chemistry, Australian National University, Canberra, ACT 0200, Australia

Received 30 June 2003; accepted 19 September 2003

Abstract

Reaction of $WH(CO)_3(\eta\text{-}C_5Me_5)$ with $IrCl(CO)_2(4\text{-}H_2NC_6H_4Me)$ affords $WIr_3(\mu\text{-}CO)_3(CO)_8(\eta\text{-}C_5Me_5)$ in low yield. A structural study reveals a WIr_2-centred plane of bridging carbonyls, in contrast to the crystal structure of $WIr_3(CO)_{11}(\eta\text{-}C_5H_5)$ (all-terminal carbonyl distribution). DFT calculations reveal an increasing proclivity to adopt an all-terminal CO disposition for clusters $MIr_3(CO)_{11}(\eta\text{-}C_5H_5)$ in the gas phase on proceeding from M = Cr to Mo and then W, consistent with structural studies in the solid state for which the tungsten-containing cluster is the only all-terminal example. Increasing electron donation from the ligands in the tungsten system (either from phosphine substitution or cyclopentadienyl permethylation) suffices to impose a plane of bridging carbonyls in the ground state structure. ^{13}C NMR fluxionality studies reveal that CO exchange mechanism(s) for $WIr_3(CO)_{11}(\eta\text{-}C_5H_5)$ and the related tetrahedral cluster $W_2Ir_2(CO)_{10}(\eta\text{-}C_5H_5)_2$ are very fast and involve all carbonyls on the clusters. DFT calculations on $MIr_3(CO)_{11}(\eta\text{-}C_5H_5)$ (M = Cr, Mo) substantiate a 'merry-go-round' mechanism for carbonyl scrambling in these systems, a result which is consistent with the scrambling behaviour seen in the NMR fluxionality studies on the W-containing congener.

Keywords: Chromium; Molybdenum; Tungsten; Iridium; Carbonyl; Cyclopentadienyl; Cluster; Density functional theory; Crystal structure; Fluxionality

1. Introduction

The complexes $M_4(CO)_{12}$ (M = Co, Rh, Ir) and their phosphine-containing derivatives are tetrahedral clusters that have been studied intensively for inter alia carbonyl ligand fluxionality [2]. Clusters of the lighter metals (Co, Rh) possess crystallographically-defined $M_4(\mu\text{-}CO)_3(CO)_9$ ground-state structures with a plane of bridging carbonyls, whereas the corresponding cluster of the heaviest metal (Ir) adopts an all-terminal carbonyl disposition in the crystallographically-observed ground state. The interconversion of these two configurations is important as a critical feature of the Cotton merry-go-round mechanism rationalizing aspects of carbonyl fluxionality in this class of cluster. The relative stability of the two configurations is clearly of interest, density functional theory (DFT) calculations on $Rh_4(\mu\text{-}CO)_3(CO)_9$ (plane-of-bridging-carbonyls) and $Rh_4(CO)_{12}$ (all-terminal) in the gas phase confirming the bridged conformation as the more stable for the rhodium cluster (by 55 kJ mol^{-1}) [3].

The tetrahedral mixed group 6-iridium clusters $MIr_3(CO)_{11}(\eta\text{-}C_5H_5)$ (M = Mo, W) are related to $Ir_4(CO)_{12}$ by (conceptual) replacement of an $Ir(CO)_3$ vertex by an isolobal $M(CO)_2(\eta\text{-}C_5H_5)$ unit. We have prepared a significant number of phosphine and isonitrile derivatives of these clusters [4–11] and, while all crystallographically-confirmed molybdenum-containing

* Corresponding author. Tel.: +61-2-6125-2927; fax: +61-2-6125-0760.
E-mail address: Mark.Humphrey@anu.edu.au (M.G. Humphrey).

0022-328X/$ - see front matter © 2003 Elsevier B.V. All rights reserved.
doi:10.1016/j.jorganchem.2003.09.026

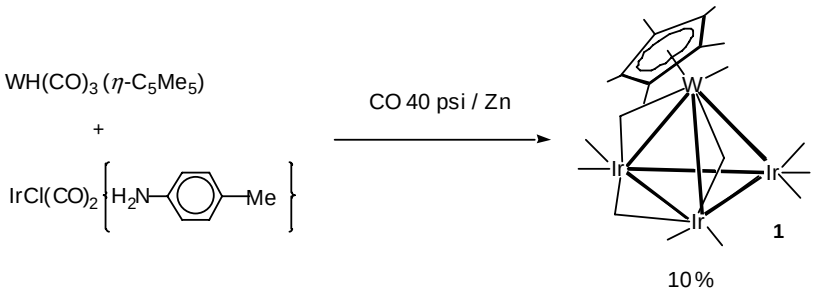

Fig. 1. Preparation of $WIr_3(\mu\text{-}CO)_3(CO)_8(\eta\text{-}C_5Me_5)$ (**1**).

clusters possess a MIr_2 plane of bridging carbonyls, crystallographically-verified tungsten-containing examples possess all-terminal or plane-of-bridging-carbonyls configurations, depending on the ligand set. We report herein the synthesis and crystallographic characterization of $WIr_3(\mu\text{-}CO)_3(CO)_8(\eta\text{-}C_5Me_5)$, for which permethylation of the cyclopentadienyl ligand is sufficient to modify the carbonyl disposition in the ground state structure, together with a DFT study exploring the proclivity of these mixed group 6-iridium tetrahedral clusters to adopt the two carbonyl ligand arrangements, and studies of ligand fluxionality at $WIr_3(CO)_{11}(\eta\text{-}C_5H_5)$ and the related tetrahedral cluster $W_2Ir_2(CO)_{10}(\eta\text{-}C_5H_5)_2$.

2. Results and discussion

2.1. Synthesis of $WIr_3(\mu\text{-}CO)_3(CO)_8(\eta\text{-}C_5Me_5)$ (1)

The mixed-metal cluster $WIr_3(\mu\text{-}CO)_3(CO)_8(\eta\text{-}C_5Me_5)$ (**1**) was prepared from the reaction of $WH(CO)_3(\eta\text{-}C_5Me_5)$ and $IrCl(CO)_2(4\text{-}H_2NC_6H_4Me)$ under several atmospheres of carbon monoxide (Fig. 1), by extending the literature procedure for the synthesis of the cyclopentadienyl-containing analogue [12]. The identity of compound **1** was confirmed by IR and ^1H NMR spectroscopy and secondary ion mass spectrometry. The solution IR spectrum shows the presence of terminal and edge-bridging carbonyl ligands. The ^1H NMR spectrum contains a sharp singlet at 2.01 ppm indicative of a pentamethylcyclopentadienyl group. The mass spectrum shows a molecular ion peak followed by consecutive loss of eight carbonyls.

It was also of interest to prepare a chromium–triiridium example, particularly as only one carbonyl-containing chromium–iridium cluster, $Cr_2Ir(\mu_3\text{-}S)(\mu\text{-}CBu^t)(CO)(PPh_3)(\eta\text{-}C_5H_5)_2$, has been reported [13]. We therefore assayed the synthetic strategy that has been successfully employed to prepare molybdenum/tungsten–triiridium clusters. The hydride precursor $CrH(CO)_3(\eta\text{-}C_5H_5)$ was prepared by the high pressure reaction of H_2 with the dimer $\{Cr(CO)_3(\eta\text{-}C_5H_5)\}_2$ following a literature procedure [14], but combining an excess of this hydride with $IrCl(CO)_2(4\text{-}H_2NC_6H_4Me)$ failed to afford any tractable products.

2.2. X-ray structural study of $WIr_3(\mu\text{-}CO)_3(CO)_8(\eta\text{-}C_5Me_5)$ (1)

A single-crystal X-ray diffraction study of $WIr_3(\mu\text{-}CO)_3(CO)_8(\eta\text{-}C_5Me_5)$ (**1**) was carried out; an ORTEP diagram is shown in Fig. 2, while selected cell data and crystallographic structure acquisition and processing parameters are collected in Table 1. The cluster contains a WIr_3 tetrahedral core geometry with the tungsten ligated by one pentamethylcyclopentadienyl group and a terminal carbonyl ligand, one iridium bearing three terminal carbonyl ligands, and the other two iridium atoms each ligated by two terminal carbonyl ligands. Three bridging carbonyls about a WIr_2 face complete the coordination. The cluster is electron precise, with 60 $[6(W) + 3 \times 9(Ir) + 5(\eta\text{-}C_5Me_5) + 11 \times 2(CO)]$ cluster valence electrons. The plane of bridging carbonyls about a WIr_2 face is in contrast to the crystallographically-reported all-terminal structures of analogous clusters with

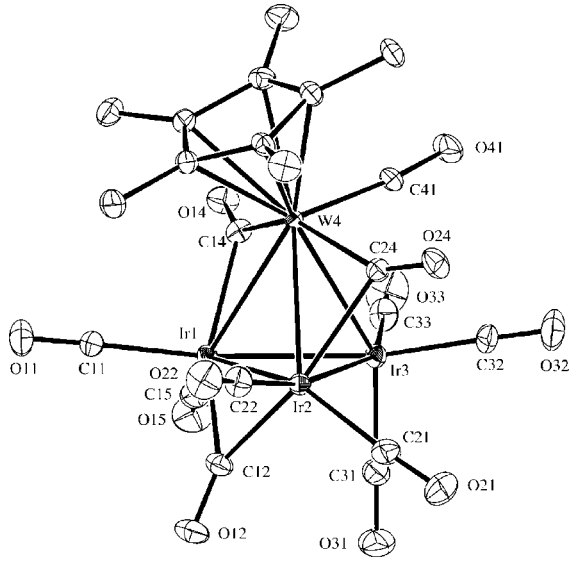

Fig. 2. ORTEP plot and atomic numbering scheme for $WIr_3(\mu\text{-}CO)_3(CO)_8(\eta\text{-}C_5Me_5)$ (**1**). Displacement ellipsoids are at the 30% probability level. Hydrogen atoms have been omitted for clarity.

Table 1
Crystal data and structure refinement details for **1**

Empirical formula	$C_{21}H_{15}Ir_3O_{11}W$
Formula weight	1203.85
Crystal size (mm)	$0.38 \times 0.11 \times 0.09$
Colour, habit	Red, plate
Crystal system	Monoclinic
Space group	$P2_1/c$
a (Å)	8.4837 (1)
b (Å)	19.2771 (2)
c (Å)	15.3878 (1)
α (°)	90
β (°)	91.86
γ (°)	90
V (Å^3)	2515.21 (4)
Z	4
D_{calc} (g cm^{-3})	3.179
μ (mm^{-1})	20.44
θ_{max} (°)	33
$N_{collected}$	68,210
$N_{aunique}$	9141
N_{obs}	5646 ($I > 3.00\sigma(I)$)
Absorption correction	Integration
T_{min}, T_{max}	0.050, 0.231
No. of parameters	326
R[a]	0.0271
R_w[b]	0.0311
S	1.08
$(\Delta/\rho)_{min}$ (e Å^{-3})	−2.98
$(\Delta/\rho)_{max}$ (e Å^{-3})	2.85

[a] $R \sum ||F_o| - |F_c|| / \sum |F_o|$.
[b] $R_w = [(\sum w|F_o| - |F_c|^2 / \sum wF_o^2)]^{1/2}$.

Table 2
Selected bond lengths (Å) and angles (°) for $WIr_3(\mu\text{-}CO)_3(CO)_8(\eta\text{-}C_5Me_5)$ (**1**)

Ir1–Ir2	2.7029(3)	Ir1–Ir3	2.7088(3)
Ir1–W4	2.8615(3)	Ir2–Ir3	2.7088(3)
Ir2–W4	2.8553(3)	Ir3–W4	2.8996(3)
W4–C401	2.310(6)	W4–C402	2.315(6)
W4–C403	2.367(6)	W4–C404	2.372(6)
W4–C405	2.359(6)	Ir1–C11	1.895(7)
Ir1–C15	1.888(7)	Ir2–C21	1.888(7)
Ir2–C22	1.893(6)	Ir3–C31	1.897(7)
Ir3–C32	1.924(7)	Ir3–C33	1.943(7)
W4–C41	1.960(6)	Ir1–C12	2.100(7)
Ir2–C12	2.105(6)	Ir1–C14	2.198(6)
W4–C14	2.110(6)	Ir2–C24	2.247(6)
W4–C24	2.104(6)		
Ir2–Ir1–Ir3	60.073(8)	Ir2–Ir1–W4	61.669(8)
Ir3–Ir1–W4	62.668(8)	Ir1–Ir2–Ir3	60.071(8)
Ir1–Ir2–W4	61.898(8)	Ir3–Ir2–W4	62.750(8)
Ir1–Ir3–Ir2	59.856(8)	Ir1–Ir3–W4	61.243(7)
Ir2–Ir3–W4	61.097(8)	Ir1–W4–Ir2	56.433(7)
Ir1–W4–Ir3	56.089(7)	Ir2–W4–Ir3	56.153(7)
Ir1–C12–O12	140.7(6)	Ir2–C12–O12	139.0(6)
Ir1–C14–O14	129.2(5)	W4–C14–O14	147.5(5)
Ir2–C24–O24	127.7(5)	W4–C24–O24	150.3(5)

methylcyclopentadienyl [15] and cyclopentadienyl [12,16] ligands and a carbonyl substitution derivative of the former with two $CNC_6H_3Me_2$-2,6 ligands [9], but a plane of bridging carbonyls about a WIr_2 face is also seen in the structure of the cyclopentadienyl-containing derivative where one of the carbonyl groups is replaced by PPh_3 [5] or $P(OMe)_3$ [17], or two of the carbonyls are replaced by $P(OPh)_3$ [7], or the methylcyclopentadienyl derivative where one carbonyl is replaced by PMe_3 [10], ligand replacements that increase electron donation to the cluster. Note that a plane of bridging carbonyls about the Ir_3 face is seen in the structures of cyclopentadienyl-containing derivatives where one of the carbonyls is replaced by PMe_3 [5] or $P(OMe)_3$ [8], or where two of the carbonyls are replaced by an Ir–Ir bridging bidentate diphosphine (bis(diphenylphosphino)methane, dppm; 1,2-bis(diphenylphosphino)ethane, dppe; bis(diphenylphosphino)acetylene, dppa) [4]. In all instances, a plane of bridging carbonyls is observed upon introduction of a sufficiently strongly electron-donating ligand. The plane of bridging carbonyls in the present structural study is therefore likely to result from the greater electron donation of the pentamethylcyclopentadienyl ligand compared to its less highly methylated cyclopentadienyl analogues. In contrast, all structurally-characterized molybdenum–triiridium clusters (with a range of cyclopentadienyl ligands and/or phosphine substitution) contain a $MoIr_2$ plane of bridging carbonyls [10,18,19].

Selected bond lengths and angles are collected in Table 2. The core bond lengths in compound **1** fall into the ranges Ir–Ir [2.7029(3)–2.7088(3); $Ir–Ir_{av} = 2.7068$ Å] and W–Ir [2.8553(3)–2.8996(3); $W–Ir_{av} = 2.8721$ Å]. Comparison to the core bond lengths of $WIr_3(CO)_{11}(\eta\text{-}C_5H_5)$ (**2**) ($Ir–Ir_{av} = 2.699$, $W–Ir_{av} = 2.824$ Å) [12] and $WIr_3(\mu\text{-}CO)_3(CO)_7(PMe_2Ph)(\eta\text{-}C_5H_5)$ ($Ir–Ir_{av} = 2.745$, $W–Ir_{av} = 2.854$ Å) [8] reveals that increasing electron density at the cluster core by permethylation of the cyclopentadienyl ligand or by substitution of PMe_2Ph for a carbonyl both result in increases in core bond lengths. As with previous structural determinations for this class of cluster, core angles are ca 60° as expected, with those at the sterically-more-congested tungsten ca 56°. CO(12) bridges symmetrically, whereas CO(14) and CO(24) are unsymmetrically arranged with d(W–C) < d(Ir–C) and indeed distorted further from a symmetrical distribution than are the corresponding carbonyls in $MoIr_3(\mu\text{-}CO)_3(CO)_8(\eta\text{-}C_5H_5)$ [19]. Terminally-bound carbonyls are unexceptional, with Ir–CO [1.888(7)–1.943(7) Å; 174.2(7)–178.6(8)°] and W–CO [1.960(6) Å; 173.2(6)°] within the expected ranges, and deviations from linearity likely to be due to packing forces.

2.3. Theoretical studies

DFT was employed to assess the proclivity for all-terminal vs plane-of-bridging-carbonyls ligand disposition in this series of clusters. In all cases, geometry optimizations on tri-bridged and unbridged MIr_3

$(CO)_{11}(\eta\text{-}C_5H_5)$ (M = Cr, Mo, W (**2**)) clusters were performed in C_s symmetry. While these calculations ultimately all led to stationary points having the desired bond connectivity, optimization of the unbridged $CrIr_3(CO)_{11}(\eta\text{-}C_5H_5)$ structure was problematic and our preliminary calculations led instead to a lower-energy structure possessing two bridging and three face-capping CO ligands (the three capped faces being those involving the unique Ir as one vertex). While this multiply-capped structure was found to be significantly higher in energy than the more 'orthodox' triply-bridged geometry (by ~0.3 eV according to VWN calculations employing type IV basis sets), its substantial stabilization relative to the unbridged $CrIr_3(CO)_{11}(\eta\text{-}C_5H_5)$ local minimum suggests that the all-terminal Cr congener of the Mo- and W-containing clusters is likely to elude laboratory isolation.

Our raw geometry optimizations, in C_s symmetry, show an almost constant energy separation between the plane-of-bridging-carbonyls and all-terminal isomers, with the all-terminal stationary point geometry lying slightly more than 1 eV higher in energy than the plane-of-bridging-carbonyls structure in each instance. The lack of any relative-energy dependence on the identity of the group 6 metal, in our VWN-optimized geometry calculations, contrasts with the consistent trend seen in the relativistically-corrected single-point calculations. The latter calculations show that, when relativistic corrections are included (and regardless of whether non-local corrections are incorporated), the stabilization of the plane-of-bridging-carbonyls isomer is greatest for M = Cr and least for M = W (see Table 3).

One shortcoming of the C_s-symmetry optimizations is that they cannot unambiguously identify the stationary points as minima. Such identification could be provided by vibrational frequency calculation; however, the numerical calculation of vibrational frequencies using the ADF program package is prohibitively computationally expensive for the 36-atom clusters of interest. As an alternative assessment of this issue, we have performed additional reoptimizations of slightly-distorted all-terminal $MIr_3(CO)_{11}(\eta\text{-}C_5H_5)$ structures in the absence of any symmetry constraints. These reoptimizations were undertaken with all geometric parameters initialized at the values optimized for the all-terminal C_s-symmetry stationary point, except that the CO ligand lying within the symmetry plane in the C_s geometry was tilted approximately 10° out of this plane. Reoptimization in this fashion showed that, while the W-containing structure spontaneously reverted to the C_s-symmetry all-terminal configuration, the Cr- and Mo-containing congeners rearranged to yield the tri-bridged structure, again with effective re-establishment of C_s symmetry. The stability of the all-terminal W-containing species in these calculations demonstrates that it is indeed a local minimum at this level of theory, while the corresponding all-terminal Cr- and Mo-containing configurations must be considered as saddle points upon their potential energy surfaces.

Our results ultimately reveal the same type of trend as Calhorda and co-workers [20,21] have reported in DFT calculations on $M_2(CO)_9$ and $M_3(CO)_{12}$ clusters, where M = Fe, Ru, or Os. In their calculations (on smaller clusters than those investigated here, with many well-characterized crystallographic structures amongst the species surveyed) they found a consistent tendency towards carbonyl bridging in Fe-containing clusters, and towards terminal carbonyl ligation in clusters dominated by Os. A countervailing trend is suggested by the DFT calculations of Besançon et al. [3] on $Rh_3M(CO)_{12}$ clusters (M = Rh, Ir): the plane-of-bridging-carbonyls isomer stationary point is favoured over the all-terminal geometry (which appears to represent a transition structure for scrambling of the bridging plane) in both cases, but *more so* when the cluster contains Ir than in the all-Rh species. The theoretical results of Besançon et al. [3], which appear to be in accordance with experimental studies on the $Rh_3M(CO)_{12}$ systems, also reveal that the bond lengths between metal atoms are habitually longer in the plane-of-bridging-carbonyls geometry than in the all-terminal geometry. This tendency is seen also in our optimizations, with the bridged M–Ir bond longer by 0.047 Å (Cr), 0.068 Å (Mo), and 0.113 Å (W) than the corresponding unbridged M–Ir bond; smaller bond contractions (typically 0.01 Å) are seen on removing the carbonyl bridge from the symmetry-equiv-

Table 3
Calculated trends in the relative energy of tri-bridged and all-terminal CO-ligated MIr_3 clusters, obtained from density functional theory calculations

$MIr_3(\mu\text{-}CO)_n(CO)_{11-n}(\eta\text{-}C_5H_5)$		E_{rel} (kJ mol^{-1})[b]		
M	n[a]	VWN	VWN + ZORA	B-LYP + ZORA
Cr	3	0	0	0
Cr	0	117	77	68
Mo	3	0	0	0
Mo	0	102	51	49
W	3	0	0	0
W	0	115	36	28

[a] Number of bridging carbonyls in the optimized geometry.
[b] Energy, expressed relative to the total energy of the lowest-energy stationary point, for single-point calculations using the indicated density functional method. In all cases, single-point calculations were performed upon the VWN-optimized geometries.

alent pair of Ir atoms. A rationale to account for this observation is that the bridging interaction increases the metal–ligand interaction at the expense of metal–metal overlap, and thereby weakens the metal–metal bond. Such an occurrence would tally with the trend towards stabilization of the all-terminal geometry, permitting more efficient metal–metal bond formation, as M is changed from Cr to Mo to W, since the greater preference towards metal–metal bonding of third-row transition metal compounds is a commonly-encountered feature of dinuclear and polynuclear transition metal complexes.

2.4. Fluxionality studies of $WIr_3(CO)_{11}(\eta\text{-}C_5H_5)$ (2) and $W_2Ir_2(CO)_{10}(\eta\text{-}C_5H_5)_2$ (3)

The ready accessibility of both plane-of-bridging-carbonyls and all-terminal isomers for **2** suggests that it may be fluxional by inter alia the merry-go-round pathway, so dynamic NMR spectra of **2** and the related tetrahedral cluster $W_2Ir_2(CO)_{10}(\eta\text{-}C_5H_5)_2$ (**3**) were acquired. The room temperature ^{13}C NMR spectrum of $WIr_3(CO)_{11}(\eta\text{-}C_5H_5)$ (**2**) in $CDCl_3$ consists of a singlet at 178.2 ppm (Fig. 3). On cooling to 156K (CD_2Cl_2/$CHFCl_2$), the spectrum splits into two broad signals that could not be fully resolved due to solvent restrictions, solubility, and other experimental problems. Similarly, the room temperature ^{13}C NMR spectrum of **3** in $CDCl_3$ consists of one averaged signal at 180.0 ppm that, on cooling to 148 K ($CDFCl_2$), splits into two broad and one sharp resonance (Fig. 4). The exchange mechanism(s) for both **2** and **3** are very fast, and appear to involve all the carbonyls on the clusters. This is in contrast to CO fluxionality at $Ir_4(CO)_{11}(L)$, for which the carbonyl *trans* to the substituted ligand is not involved in exchange either by merry-go-round or face-centred exchange mechanisms [22]. The ^1H NMR spectrum for **3** at 148 K reveals one broad signal for the cyclopentadienyl ligands (5.18 ppm, $CDFCl_2$), reinforcing the suggestion that exchange is very fast.

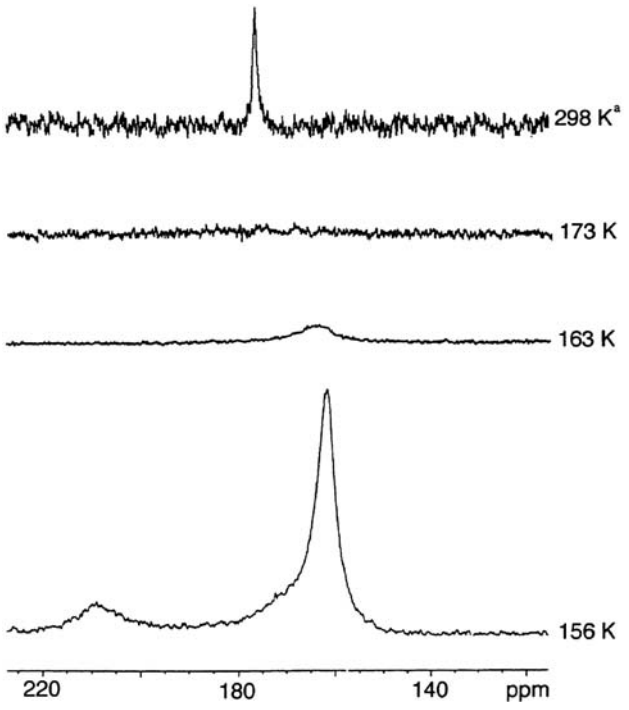

Fig. 3. Variable temperature ^{13}C NMR spectroscopic study of $WIr_3(CO)_{11}(\eta\text{-}C_5H_5)$ (**2**) in $CD_2Cl_2/CHFCl_2$ ([a] in $CDCl_3$).

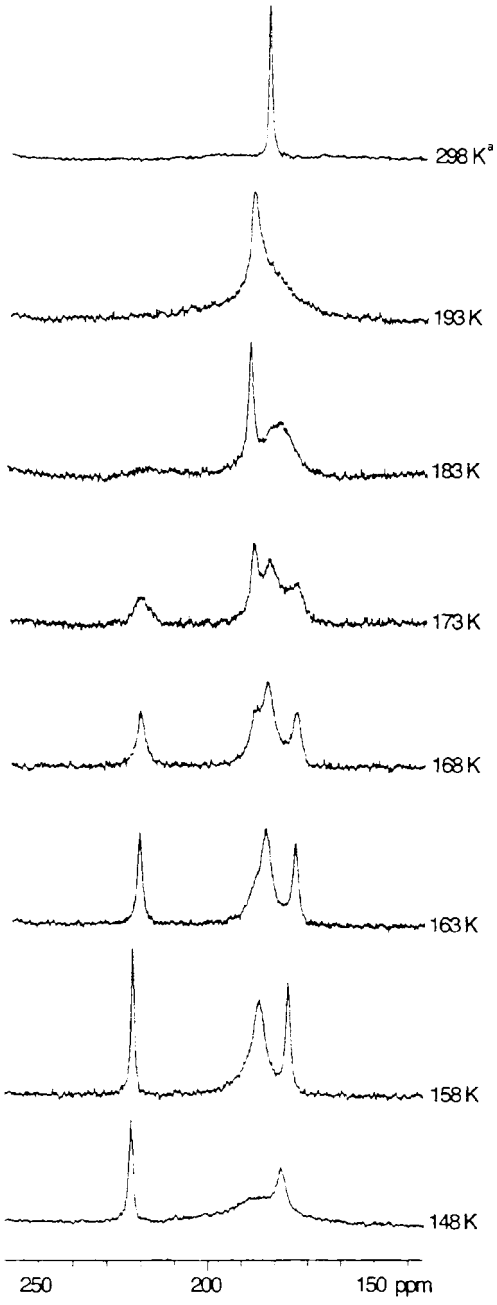

Fig. 4. Variable temperature ^{13}C NMR spectroscopic study of $W_2Ir_2(CO)_{10}(\eta\text{-}C_5H_5)_2$ (**3**) in $CDFCl_2$ ([a] in $CDCl_3$).

2.5. Discussion

The experimental studies described herein have shown that permethylating a cyclopentadienyl ligand results in the carbonyl disposition in the crystallographically-observed ground-state structure of the tungsten–triiridium clusters proceeding from all-terminal to plane-of-bridging-carbonyls, a similar result to that observed on introduction of electron-donating phosphine ligands, and in contrast to results with molybdenum–triiridium clusters for which plane-of-bridging-carbonyls is always observed. We have also shown that the chromium–triiridium analogue is not accessible under similar experimental conditions. DFT calculations support the experimental observation of an increasing proclivity for an all-terminal configuration on introduction of the heaviest metal, the all-terminal geometry being increasingly stabilized on proceeding from Cr to Mo to W.

We have previously reported fluxionality studies of $WIr_3(\mu\text{-}CO)_3(CO)_7(L)(\eta\text{-}C_5H_5)$ ($L = PPh_3$, PMe_3 [23]), $WIr_3(CO)_{10}(CNBu^t)(\eta\text{-}C_5H_5)$ [9], and $WIr_3(\mu\text{-}CO)_3(CO)_6(L_2)(\eta\text{-}C_5H_5)$ ($L_2 =$ dppm, dppe [8]). Whereas the isonitrile-containing cluster was highly fluxional (cooling to 143 K revealed broadening of the ^{13}C NMR resonances only), low temperature limiting spectra of the phosphine-containing clusters could be obtained, the fluxionality being shown to proceed via the merry-go-round process as a key step. The ready accessibility of both plane-of-bridging-carbonyls and all-terminal carbonyl dispositions from ligand replacement at **2** is consistent with its highly fluxional character and suggests involvement of these two forms in carbonyl fluxionality, perhaps via the merry-go-round process similar to its phosphine-substituted derivatives.

Some insight into the mechanism of carbonyl fluxionality in **2** is in fact available from our DFT calculations. While (in our calculations) the W-containing structure itself does not undergo spontaneous rearrangement from the all-terminal to the tri-bridged configuration when symmetry constraints are removed, such rearrangement is seen for the Cr- and Mo-containing congeners. Besançon et al. [3] have verified, by comparison of theoretical and experimental activation volumes as well as from interpretation of the ^{13}C NMR spectra, that the all-terminal geometry represents the transition state to CO scrambling (via a 'merry-go-round' mechanism) in tri-bridged $MRh_3(CO)_{12}$ ($M = Rh$, Ir). We may assume here that the all-terminal geometry similarly corresponds to the transition state for rearrangement of the carbonyl ligands in MIr_3-containing systems for which the tri-bridged configuration is the global minimum. From the observed ligand rearrangement in our no-symmetry optimizations, it is apparent that the 'tri-bridged $\leftrightarrow$ all-terminal $\leftrightarrow$ tri-bridged' interconversion in our calculations on Cr- and Mo-containing clusters also occurs via a 'merry-go-round' mechanism and thus allows for the complete scrambling of all carbonyls. This tendency is mechanistically consistent with the equivalence of all carbonyls noted above for **2** at temperatures above 156 K.

3. Experimental

3.1. General conditions

The reaction solvents CH_2Cl_2 and thf were analytical reagent (AR) grade and were dried over CaH_2 and sodium/benzophenone, respectively, and distilled under nitrogen. Petrol refers to a fraction of boiling range 60–80 °C. Literature procedures (or minor modifications thereof) were used to synthesize $IrCl(CO)_2$(*p*-toluidine) [24], $WH(CO)_3(\eta\text{-}C_5Me_5)$ [25], $WIr_3(CO)_{11}(\eta\text{-}C_5H_5)$ (**2**) [12] and $W_2Ir_2(CO)_{10}(\eta\text{-}C_5H_5)_2$ (**3**) [12]; ^{13}CO-enriched samples were prepared by stirring solutions of the clusters in CH_2Cl_2 under 1.2 atm ^{13}CO at 60 °C for 48 h (**2**) or at room temperature for 60 h (**3**). The product **1** was purified by thin-layer chromatography on 20×20 cm glass plates coated with Merck GF_{254} silica gel (0.5 mm). The infrared spectrum was recorded on a Perkin–Elmer System 2000 FT-IR with CaF_2 solution cells as a solution in cyclohexane (AR grade); spectral frequencies are recorded in cm^{-1}. The ^1H NMR spectra were recorded in $CDCl_3$ (Cambridge Isotope Laboratories) using a Varian Gemini-300 spectrometer at 300 MHz and referenced to residual $CHCl_3$ at 7.24 ppm. The ^{13}C NMR spectra were recorded in $CDCl_3$, CD_2Cl_2 (Cambridge Isotope Laboratories) and $CDFCl_2$ [26]. The unit resolution SI mass spectrum was recorded using a VG Autospec instrument at the Research School of Chemistry, Australian National University, and data are reported in the form: m/z (assignment, relative intensity). The elemental microanalysis was carried out by the Microanalysis Service Unit in the Research School of Chemistry, ANU.

3.2. Preparation of $WIr_3(\mu\text{-}CO)_3(CO)_8(\eta\text{-}C_5Me_5)$ (1)

A solution of freshly prepared $WH(CO)_3(\eta\text{-}C_5Me_5)$ (ca 0.56 mmol) in CH_2Cl_2 (25 mL) was added to $IrCl(CO)_2$(*p*-toluidine) (186 mg, 0.478 mmol) and acid-washed granular zinc (ca 1.0 g) in a nitrogen filled, 250 mL glass pressure bottle. The bottle was pressurized to 40 psi with carbon monoxide and placed in an oil bath at 60 °C for 16 h with stirring. The oil bath was then cooled to room temperature, the glass pressure bottle vented and the solvent removed in vacuo. The red solid residue was extracted with CH_2Cl_2 (ca 10 mL) and the resultant solution applied to preparative TLC plates. Elution with CH_2Cl_2/petrol (1/4) gave two bands. Band 1 was pink ($R_f = 0.83$) and Band 2 was yellow ($R_f = 0.48$). Band 1 decomposed on the plate and was

not collected. The contents of band 2 were recrystallized from CH_2Cl_2/MeOH by liquid diffusion at 276K to afford dark orange crystals identified as $WIr_3(\mu\text{-}CO)_3(CO)_8(\eta\text{-}C_5Me_5)$ (**1**) (60 mg, 0.049 mmol, 10%). Anal. Found: C, 21.46; H, 1.33%. $C_{21}H_{15}Ir_3O_{11}W$ Calcd.: C, 20.95; H, 1.26%. IR (*c*-C_6H_{12}): ν(CO) 2088 m, 2054 m, 2047 vs, 2026 m, 2003 m, 1917 w, 1863 m, 1801 vw, 1773 w cm^{-1}. ^1H NMR ($CDCl_3$): δ 2.01 (s, 15H, C_5Me_5) ppm. MS: 1204 ($[M]^+$, 22), 1176 ($[M-CO]^+$, 35), 1148 ($[M-2CO]^+$, 37), 1120 ($[M-3CO]^+$, 100), 1092 ($[M-4CO]^+$, 48), 1064 ($[M-5CO]^+$, 20), 1036 ($[M-6CO]^+$, 10), 1008 ($[M-7CO]^+$, 25), 980 ($[M-8CO]^+$, 7).

3.3. Attempted preparation of $CrIr_3(\mu\text{-}CO)_3(CO)_8(\eta\text{-}C_5H_5)$

The precursor $CrH(CO)_3(\eta\text{-}C_5H_5)$ was prepared from $\{Cr(CO)_3(\eta\text{-}C_5H_5)\}_2$ (710 mg, 1.76 mmol) under 400 psi H_2 in thf (70 mL) at room temperature following a literature procedure [14]. Handling of these air-sensitive compounds, in particular the loading and dismantling of the autoclave, was carried out under an argon atmosphere in a glove box. The reaction solution was divided equally between two Schlenk tubes, and the contents of one tube were taken to dryness in vacuo. The residue was dissolved in CH_2Cl_2 (80 mL) and transferred to a 250 mL glass pressure bottle, to which was added $IrCl(CO)_2$(*p*-toluidine) (100 mg, 0.255 mmol) and granular zinc (ca 0.5 g). The bottle was flushed with carbon monoxide, then pressurized to 40 psi and heated (with stirring) in an oil bath at 60 °C for 17 h. After cooling to room temperature, the bottle was carefully vented, the solution filtered and taken to dryness. The residue was extracted into a small volume (ca 3 mL) of CH_2Cl_2 and applied to preparative TLC plates. Elution with CH_2Cl_2/petrol (2/5) failed to afford any tractable products.

3.4. X-ray crystallographic study

The crystal and refinement data for compound **1** are summarized in Table 1. Crystals suitable for X-ray structural analyses were grown by liquid diffusion from CH_2Cl_2/MeOH at 276 K. A single crystal was mounted on a fine glass capillary, and data collected on a Nonius Kappa CCD diffractometer at 200 K using graphite monochromated Mo Kα ($\lambda = 0.71069$ Å). The unit cell parameters were obtained by least squares refinement [27] of 56490 reflections with $3 \leqslant \theta \leqslant 33°$. The reduced data [27] were corrected for absorption using numerical methods [28] implemented from within maXus [29]; equivalent reflections were merged. The structure was solved by direct methods and expanded using Fourier techniques [30] within the software package maXus.

The crystallographic asymmetric unit for **1** consists of one molecule with all atoms in general positions. All non-hydrogen atoms were refined with anisotropic displacement parameters. H atoms attached to C atoms were included in idealized positions and ride on the atoms to which they are bonded. The methyl H atoms were oriented to best-fit peaks observed in a difference electron density map. The final cycles of matrix least squares refinement were based on 5646 reflections and converged to $R = 0.027$ and $R_W = 0.031$. The largest peaks in the final difference electron map are located near Ir and W atoms.

3.5. Theoretical methods

Density functional theory calculations were performed on Linux-based Pentium IV 1.7–2.8 GHz computers using the Amsterdam Density Functional (ADF) program, version ADF 2000 [31], developed by Baerends et al. [32–36]. Some subsequent calculations, performed using ADF2002, were executed in parallel mode on the AlphaSever supercomputer housed at the ANU Supercomputer Facility and operated under the Australian Partnership for Advanced Computing.

Calculations on $MIr_3(CO)_{11}(\eta\text{-}C_5H_5)$ structures were performed in C_s symmetry, or in the absence of symmetry constraints. Electrons in orbitals up to and including 1s {C, O}, 2p {Cr}, 3d {Mo} and 4d {W, Ir} were treated in accordance with the frozen-core approximation. Geometry optimizations employed the local density approximation (LDA) to the exchange potential [37,38], and the correlation potential of Vosko et al. [39], with a triple-ζ-plus-polarization quality Slater type orbital basis set for each atom; these basis sets are described as 'Type IV' for ADF2000 and as 'TZP' for ADF2002. All calculations were spin-restricted.

Non-local and relativistic corrections to the local density approximation were effected through single-point calculations employing the B-LYP non-local exchange and correlation functionals and the ZORA scalar relativistic correction, using basis sets analogous to those employed in the geometry optimization calculations. We have previously found [10], as have others [3], that the VWN parametrization of the local density approximation delivers significantly better metal–metal and metal–ligand bond lengths for carbonylated metal clusters than are attained when non-local functionals (e.g., B-LYP) are employed for optimization: nevertheless, incorporation of non-local and relativistic corrections is generally considered to yield more accurate total and relative energies.

4. Supplementary material

Crystallographic data for the structural analysis have been deposited with the Cambridge Crystallographic Data Centre, CCDC no. 211613 (**1**). Copies of this in-

formation may be obtained, free of charge, from the Director, CCDC, 12 Union Road, Cambridge CB2 1E2, UK (fax: +44-1223-336033; e-mail: deposit@ccd. cam.ac.uk or www: http://www.ccdc.cam.ac.uk).

Acknowledgements

We thank the Australian Research Council (ARC) for financial support and Johnson-Matthey Technology Centre for the generous loan of iridium salts. MGH holds an ARC Australian Senior Research Fellowship, NTL held an Australian Postgraduate Award, and AJU held an ANU Honours Year Scholarship.

References

[1] Part 25: A.J. Usher, M.G. Humphrey, A.C. Willis, J. Organomet. Chem. 682 (2003) 41.
[2] D.F. Shriver, H.D. Kaesz, R.D. Adams, The Chemistry of Metal Cluster Complexes, VCH, New York, 1990.
[3] K. Besançon, G. Laurenczy, T. Lumini, R. Roulet, R. Bruyndonckx, C. Daul, Inorg. Chem. 37 (1998) 5634.
[4] J. Lee, M.G. Humphrey, D.C.R. Hockless, B.W. Skelton, A.H. White, Organometallics 12 (1993) 3468.
[5] S.M. Waterman, M.G. Humphrey, V.-A. Tolhurst, D.C.R. Hockless, B.W. Skelton, A.H. White, Organometallics 15 (1996) 934.
[6] N.T. Lucas, I.R. Whittall, M.G. Humphrey, D.C.R. Hockless, M.P.S. Perera, M.L. Williams, J. Organomet. Chem. 540 (1997) 147.
[7] S.M. Waterman, M.G. Humphrey, D.C.R. Hockless, J. Organomet. Chem. 555 (1998) 25.
[8] S.M. Waterman, M.G. Humphrey, D.C.R. Hockless, J. Organomet. Chem. 565 (1998) 81.
[9] S.M. Waterman, M.G. Humphrey, D.C.R. Hockless, J. Organomet. Chem. 579 (1999) 75.
[10] N.T. Lucas, J.P. Blitz, S. Petrie, R. Stranger, M.G. Humphrey, G.A. Heath, V. Otieno-Alego, J. Am. Chem. Soc. 124 (2002) 5139.
[11] A.J. Usher, M.G. Humphrey, A.C. Willis, J. Organomet. Chem. 678 (2003) 72.
[12] J.R. Shapley, S.J. Hardwick, D.S. Foose, G.D. Stucky, J. Am. Chem. Soc. 103 (1981) 7383.
[13] A.A. Pasynskii, I.L. Eremenko, V.R. Zalmanovitch, V.V. Kaverin, B. Orazsakhatov, S.E. Nefedov, O.G. Ellert, V.M. Novotortsev, A.I. Yanovsky, Y.T. Struchkov, J. Organomet. Chem. 414 (1991) 55.
[14] G.J. Kubas, G. Kiss, C.D. Hoff, Organometallics 10 (1991) 2870.
[15] E.G.A. Notaras, N.T. Lucas, J.P. Blitz, M.G. Humphrey, J. Organomet. Chem. 631 (2001) 143.
[16] M.R. Churchill, J.P. Hutchinson, Inorg. Chem. 20 (1981) 4112.
[17] S.M. Waterman, M.G. Humphrey, D.C.R. Hockless, J. Organomet. Chem. 582 (1999) 310.
[18] N.T. Lucas, I.R. Whittall, M.G. Humphrey, Acta Crystallogr. C 58 (2002) m249.
[19] M.R. Churchill, Y.-J. Li, J.R. Shapley, D.S. Foose, W.S. Uchiyama, J. Organomet. Chem. 312 (1986) 121.
[20] E. Hunstock, C. Mealli, M.J. Calhorda, J. Reinhold, Inorg. Chem. 38 (1999) 5053.
[21] E. Hunstock, M.J. Calhorda, P. Hirva, T.A. Pakkanen, Organometallics 19 (2000) 4624.
[22] G.F. Stuntz, J.R. Shapley, J. Am. Chem. Soc. 99 (1977) 607.
[23] S.M. Waterman, M.G. Humphrey, Organometallics 18 (1999) 3116.
[24] U. Klabunde, Inorg. Synth. 15 (1974) 82.
[25] A.R. Manning, P. Hackett, R. Birdwhistell, Inorg. Synth. 28 (1990) 148.
[26] J.S. Siegel, F.A.L. Anet, J. Org. Chem. 53 (1988) 2629.
[27] Z. Otwinowski, W. Minor, in: C.W. Carter, R.M. Sweet (Eds.), Methods in Enzymology, Academic Press, New York, 1997, p. 255.
[28] P. Coppens, in: F.R. Ahmed, S.R. Hall, C.P. Huber (Eds.), Crystallographic Computing, Munksgaard, Copenhagen, 1970, p. 307.
[29] S. Mackay, C.J. Gilmore, C. Edwards, N. Stewart, K. Shankland, maXus: computer program for the solution and refinement of crystal structures, Nonius, The Netherlands, MacScience, Japan, and The University of Glasgow, UK, 1999.
[30] P.T. Beurskens, G. Admiraal, G. Beurskens, W.P. Bosman, R. de Gelder, R. Israel, J.M.M. Smits, The DIRDIF-94 Program System, Technical Report of the Crystallography Laboratory, University of Nijmegen, The Netherlands, 1994.
[31] E.J. Baerends, A. Bérces, C. Bo, P.M. Boerrigter, L. Cavallo, L. Deng, R.M. Dickson, D.E. Ellis, L. Fan, T.H. Fischer, C. Fonseca Guerra, S.J.A. van Gisbergen, J.A. Groeneveld, O.V. Gritsenko, F.E. Harris, P. van den Hoek, H. Jacobsen, G. van Kessel, F. Kootstra, E. van Lenthe, V.P. Osinga, P.H.T. Philipsen, D. Post, C. Pye, W. Ravenek, P. Ros, P.R.T. Schipper, G. Schreckenbach, J.G. Snijders, M. Sola, D. Swerhone, G. te Velde, P. Vernooijs, L. Versluis, O. Visser, E. van Wezenbeek, G. Wiesenekker, S.K. Wolff, T.K. Woo, T. Ziegler, ADF primary reference, 2000.01, 2000.
[32] E.J. Baerends, D.E. Ellis, P. Ros, Chem. Phys. 2 (1973) 42.
[33] E.J. Baerends, P. Ros, Chem. Phys. 2 (1973) 52.
[34] E.J. Baerends, P. Ros, Int. J. Quantum Chem. s12 (1978) 169.
[35] L. Versluis, T.J. Ziegler, J. Chem. Phys. 88 (1988) 322.
[36] G. te Velde, E.J. Baerends, J. Comput. Chem. 99 (1992) 84.
[37] R.G. Parr, W. Yang, Density Functional Theory of Atoms and Molecules, Oxford University Press, New York, 1989.
[38] T. Ziegler, Chem. Rev. 91 (1991) 1.
[39] S.H. Vosko, L. Wilk, M. Nusair, Can. J. Phys. 58 (1980) 1200.